A Numerical Method to Evaluate Power System Global Stability Determined by Limit Cycle

Masayuki Watanabe, *Student Member, IEEE*, Yasunori Mitani, *Member, IEEE*, and Kiichiro Tsuji, *Member, IEEE*

***Abstract*—This paper presents a method to investigate a global stability in a multi-machine power system with multiple dominant power oscillation modes. The global stability boundary formed by an unstable limit cycle is predicted by means of Hopf bifurcation theory. The authors have investigated a numerical method to analyze the nonlinear characteristics in power systems by acquiring the power swing data where the coefficients of nonlinear polynomial terms are determined by the least squares method. A modified method has been also developed for the application to large-scale multi-machine power systems with longitudinally interconnected configuration. Numerical examples illustrate that the influence of the modal interaction on the nonlinear structure of the power system as well as the Hopf bifurcation characteristics can be evaluated by the proposed method.**

***Index Terms*—Bifurcation, limit cycles, nonlinear systems, power system stability.**

I. Introduction

A POWER system is a dynamic system, which includes several kinds of nonlinear elements. Transient stability is a typical example originated in the power of swing equation, which is a sine function of rotor angle. On the other hand, the use of nonlinear analysis method based on Hopf bifurcation theory [1], [2] tells us the existence and the stability of a limit cycle around an operating point. It has been investigated in the literatures so far that the structure of limit cycles results from some combination of AVR and the system parameter [3], the nonlinearity of damping coefficient [4], the effect of induction machine load [5] and oscillatory solutions of augmented swing equations [6].

In this paper the power system global stability formed by an unstable limit cycle, is evaluated. The limit cycle can be detected based on Hopf bifurcation theory. The structure of limit cycles can be calculated by analyzing the differential equations describing the whole system. The bifurcation phenomena in power systems have been investigated in detail [7]–[9] by using a general software for nonlinear analysis [10]. However, in general nonlinear system analysis in a large system holds many unresolved problems. A direct approach to analyze the nonlinearity of a high order system usually makes little sense since it displays fragmentary information. Therefore, it becomes important to simplify the problem by finding out some available features in the large system and to carry out analysis based on it. The authors have presented a numerical method of analyzing the stability region in power systems by approximating the nonlinear characteristics near the Hopf bifurcation based on the observation of the power swing after some perturbation [11]. The approximate model relaxes the constraint resulting from a large system scale since the bifurcations are analyzed based on the approximate model, in which parameters can be determined by observing the power swing of the original model. This method can detect the stability of the limit cycle and the stability boundary near the Hopf bifurcation correctly. In addition, this method does not require trial and error like using a power system simulation package for detecting the stability boundary. Applying to a one-machine and infinite bus system has demonstrated the effectiveness of this method so far [11].

In multi-machine power systems, multiple swing modes exist. When an electro-mechanical mode with a low-frequency is dominant among the power swings, the dynamics of the dominant mode is almost equivalent to that of a one-machine and infinite bus system. In this case it is demonstrated that a model with a single nonlinear vibration mode effectively predicts the characteristics of a limit cycle. However, the limit cycle occasionally bifurcates with changing its stability in the case that some quasidominant modes exist in a multi-machine system, and then the evaluation of the global stability by using the single vibration model has a large margin of error. Thus, a modified model is developed to include the interaction between oscillatory modes. The swing equations of two generators significantly participating in the dominant power swing modes are approximated by a nonlinear coupled vibration model. The bifurcation characteristics and the unstable limit cycle around an operating point are investigated numerically based on the approximate model. Some numerical analyses demonstrate the effectiveness of the proposed method.

II. Hopf Bifurcation and Power System Stability

Consider a nonlinear dynamical system described by the following equation:

$$\dot{\boldsymbol{x}} = f(\boldsymbol{x}, p), \quad \boldsymbol{x} \in \mathbf{R}^n, \quad p \in \mathbf{R} \tag{1}$$

where p is a parameter. A value of the parameter $p = p_0$ at which the vector field f loses its structural stability is called a bifurcation point. If Df (the linearization of f at $(\boldsymbol{x}_0, p_0)$) has a simple pair of pure imaginary eigenvalues at $p = p_0$, with all other eigenvalues lying off the imaginary axis, this bifurcation is called Hopf bifurcation. The orbit structure near $(\boldsymbol{x}_0, p_0)$ can

Manuscript received February 16, 2004. Paper no. TPWRS-00516-2003.

M. Watanabe and Y. Mitani are with Faculty of Engineering, Kyushu Institute of Technology, Fukuoka, Japan (e-mail: watanabe@ele.kyutech.ac.jp; mitani@ele.kyutech.ac.jp).

K. Tsuji is with Graduate School of Engineering, Osaka University, Osaka, Japan (e-mail: tsuji@pwr.eng.osaka-u.ac.jp).

Digital Object Identifier 10.1109/TPWRS.2004.836205

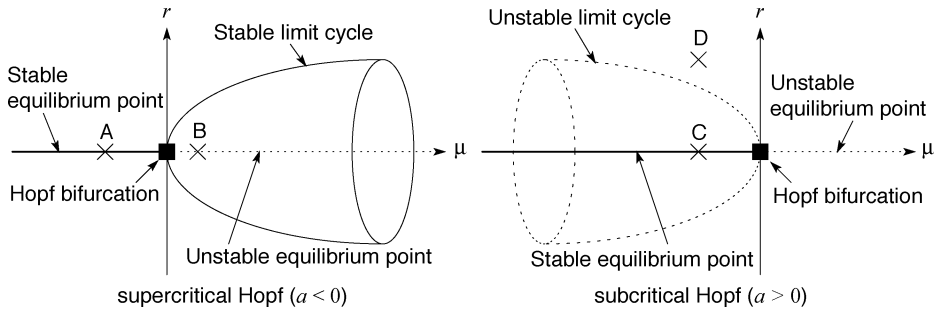

Fig. 1. Bifurcation diagrams.

be described by (1) restricted to the center manifold [2], and the vector field on the center manifold has the following form:

$$\begin{bmatrix}\dot{y}_1\\ \dot{y}_2\end{bmatrix}=\begin{bmatrix}\Re\lambda(\mu) & -\Im\lambda(\mu)\\ \Im\lambda(\mu) & \Re\lambda(\mu)\end{bmatrix}\begin{bmatrix}y_1\\ y_2\end{bmatrix}+\begin{bmatrix}f^1(y_1,y_2,\mu)\\ f^2(y_1,y_2,\mu)\end{bmatrix} \quad (2)$$

where f^1 and f^2 are nonlinear functions of y_1 and y_2, μ is a parameter, and $\lambda(\mu)=\alpha(\mu)+j\omega(\mu)$ are eigenvalues of the corresponding linear system of the vector field. In order to analyze the dynamics, (2) needs to be simplified and cast into its normal form [2] as follows:

$$\begin{bmatrix}\dot{y}_1\\ \dot{y}_2\end{bmatrix}=\begin{bmatrix}\alpha(\mu) & -\omega(\mu)\\ \omega(\mu) & \alpha(\mu)\end{bmatrix}\begin{bmatrix}y_1\\ y_2\end{bmatrix}+\begin{bmatrix}a\left(y_1^3+y_1y_2^2\right)-b\left(y_1^2y_2+y_2^3\right)\\ a\left(y_1^2y_2+y_2^3\right)+b\left(y_1^3+y_1y_2^2\right)\end{bmatrix}+\mathcal{O}(5). \quad (3)$$

In polar coordinates, (3) is given by

$$\begin{aligned}\dot{r}&=(d\mu+ar^2)r\\ \dot{\theta}&=\omega+c\mu+br^2\end{aligned} \quad (4)$$

where a, b, c, and d are constants determined by the system structure. If $d\neq 0$, there is a bifurcation at $\mu=0$. Since the first equation does not depend on θ, we see immediately that there are periodic orbits, $r=\sqrt{-d\mu/a}$. The bifurcation is said to be subcritical if the periodic solution is unstable and supercritical if it is stable. Fig. 1 shows an example of bifurcation diagrams when $d>0$.

In a power system, the Hopf bifurcation and limit cycles appear depending on the parameter values of excitation systems. The Hopf bifurcation theory is applicable to the system with the instability of a dominant mode. The mode becomes unstable as the power flow of the system increases, which corresponds to the increase of a parameter μ in Fig. 1. In this paper, the global stability formed by the unstable limit cycle in longitudinally interconnected power systems is investigated on $\delta-\omega$ phase plane.

When a power system has a supercritical Hopf bifurcation, a stable limit cycle exists around the unstable equilibrium point as shown in Fig. 1. Usually, the system is operated at a stable equilibrium point, for example, at point A in Fig. 1. However, even if operated at point B, the system does not lose the synchronization and is kept to operate with a sustained oscillation, since the system trajectory is trapped by the stable limit cycle.

On the other hand, when the system has a subcritical Hopf bifurcation, an unstable limit cycle exists around the stable equilibrium point. And this limit cycle forms a global stability boundary. If the system state moves to point D, that is, the outside of the limit cycle by a large disturbance when the system is operated at stable equilibrium point C, the system trajectory is distracted from the limit cycle and finally the generator loses the synchronization. Thus, the inner area of the unstable limit cycle corresponds to the stable region. The region occasionally can be much narrower than that calculated by the classical transient stability analysis method [3], [11].

Accordingly, it is important in stability analysis to grasp the property of the limit cycle around the operating point when the system condition is near the Hopf bifurcation point. In particular the unstable limit cycle affects the global stability. In the subsequent sections emphasis is placed on the numerical analysis of bifurcation characteristics in power systems.

III. A Nonlinear Vibration Model With a Single Mode for Hopf Bifurcation Analysis

The power swing equations of generators in an n-machine system are represented by [12]

$$\begin{aligned}M_i\dot{\omega}_i&=-D_i(\omega_i-1)+P_{mi}-P_{ei}\\ \dot{\delta}_i&=\omega_r(\omega_i-1)\end{aligned} \quad (5)$$

where $i=1,2,\cdots,n$, ω is the angular velocity, δ is the rotor angle, M is the inertia constant, D is the damping coefficient, P_m is the mechanical input to the generator, P_e is the electrical output, and $\omega_r=120\pi$ is the rated angular velocity. The effect of other generators and controllers is included in only P_{ei} by assuming that their responses are sufficiently faster than the responses of dominant modes. And in this system suppose that the specific mode associated with power oscillation becomes unstable with variation of a parameter like the loading condition. Here, select one generator (number j) significantly participating in the critical dominant oscillation mode. This is obtained by calculating the linear participation factor, which is defined in [13]. The participation factor p_{ki} represents a measure of the participation of the kth machine state in the trajectory of the ith mode. It is given by

$$p_{ki}=u_{ki}v_{ik} \quad (6)$$

where $\boldsymbol{u}_i$ and $\boldsymbol{v}_i$ are right and left eigenvectors, respectively. Then the generator swing equations are represented by

$$\begin{aligned}\dot{x}_1&=\frac{\omega_r}{M_j}\left(-D_j(\omega_j-1)+P_{mj}-P_{ej}\right)\\ &\equiv Y\end{aligned} \quad (7)$$

$$\dot{x}_2=x_1 \quad (8)$$

where $x_1=\omega_r(\omega_j-1)$, $x_2=\delta_j-\delta_{j0}$ [δ_{j0} is the generator j angle at the equilibrium point]. Here, a numerical method to approximate these equations by polynomial of x_1 and x_2 is derived

[14]. The right hand side of (7) Y is represented by a polynomial function of x_1 and x_2

$$\begin{aligned}\dot{x}_1 &\approx k_1x_1 + k_2x_2 + k_3x_1^2 + k_4x_2^2 + k_5x_1x_2 \\ &\quad + k_6x_1^3 + k_7x_2^3 + k_8x_1^2x_2 + k_9x_1x_2^2 \\ &= \sum_{i=1}^{9} k_iX_i \qquad (9)\\ \dot{x}_2 &= x_1 \qquad (10)\end{aligned}$$

where X_i is the function of x_1 and x_2. The coefficients k_i can be evaluated by applying the least squares method [15] to the time series data sets of P_{ej}, δ_j and ω_j after a small disturbance. The sum of the squared prediction errors of the N samples is

$$e^2 = \sum_{j=1}^{N}\left[Y_j - \sum_{i=1}^{9} k_iX_{ij}\right]^2 \qquad (11)$$

where Y_j and X_{ij} are the values of Y and X_i to the jth sample, respectively. The parameters k_i which minimize e^2 are given by the solution of the following normal equations:

$$A\boldsymbol{k} = \boldsymbol{b} \qquad (12)$$

where

$$A_{ih} = \sum_{j=1}^{N} X_{hj}X_{ij}, \quad b_i = \sum_{j=1}^{N} Y_jX_{ij}.$$

The nonlinear characteristics can be evaluated by using the model if the approximation is satisfactory.

The stability of the equilibrium point changes at $k_1 = 0$, that is, $k_1 = 0$ corresponds to the Hopf bifurcation point. When the coefficients k_i of approximate model are calculated, the Hopf bifurcation characteristics are determined by the sign of a represented by the following equation [11]:

$$a = \frac{k_5(k_2k_3 - k_4) - 3k_2^2k_6 + k_2k_9}{4k_2}. \qquad (13)$$

When $a > 0$, the system has a subcritical Hopf bifurcation, that is, an unstable limit cycle exists, while if $a < 0$, the bifurcation is supercritical as shown in Fig. 1. And the size of a limit cycle is determined by [11]

$$\begin{aligned}x_1 &= \sqrt{\frac{k_1k_2}{a}}\sin\left(\theta + \frac{\pi}{4}\right)\\ x_2 &= \sqrt{\frac{-k_1}{a}}\sin\left(\theta + \frac{3\pi}{4}\right). \qquad (14)\end{aligned}$$

In the case of a subcritical Hopf bifurcation, the unstable limit cycle forms a global stability boundary, which can be evaluated by the maximum value of x_1 and x_2. The derivation of (13) and (14) is given in the Appendix.

IV. A Coupled Vibration Model With Considering the Modal Interaction

In a multi-machine power system multiple swing modes exist and interact with each other. The single vibration model described above is applicable when a specific oscillatory mode becomes unstable as the power flow increases and when the influence of the other modes on this one is negligible. However, when some modes affect the dominant mode, the modeling error becomes large as shown in Sections V and VI. In this section the method is extended so as to include the influence of an additional dominant mode.

Here, a coupled vibration model with third order of polynomial is considered since the Hopf bifurcation is significantly associated with up to third order nonlinearity. The first vibration model corresponds to the dominant mode that becomes unstable as the power flow increases, while the other corresponds to the second dominant mode. Two generators which contribute to these two modes are selected, while another generator is used as the reference of the rotor angle. The dynamics of the model is represented by

$$\begin{aligned}\dot{x}_1 &= \sum_{i,j,k,l} a_{ijkl}x_1^ix_2^jx_3^kx_4^l\\ \dot{x}_2 &= x_1\\ \dot{x}_3 &= \sum_{i,j,k,l} b_{ijkl}x_1^ix_2^jx_3^kx_4^l\\ \dot{x}_4 &= x_3 \qquad (15)\end{aligned}$$

where $i = 0, \cdots, 3$, $j = 0, \cdots, 3 - (i + k + l)$, $k = 0, \cdots, 3 - (i + j + l)$, $l = 0, \cdots, 3 - (i + j + k)$, $x_1 = \omega_r(\omega_1 - \omega_s)$, $x_2 = \delta_1 - \delta_s - (\delta_{1e} - \delta_{se})$, $x_3 = \omega_r(\omega_2 - \omega_s)$, $x_4 = \delta_2 - \delta_s - (\delta_{2e} - \delta_{se})$, $a_{0000} = b_{0000} = 0$. $\omega_r = 120\pi$ is the rated angular velocity, subscript s denotes the reference generator, and subscript e denotes the initial value for the generator rotor angle. The coefficients a_{ijkl} and b_{ijkl} are determined by the least squares method, where the subscripts $ijkl$ correspond to the order of state variables.

Here, the Jacobian of the coupled vibration model (15) is

$$A = \begin{bmatrix} a_{1000} & a_{0100} & a_{0010} & a_{0001}\\ 1 & 0 & 0 & 0\\ b_{1000} & b_{0100} & b_{0010} & b_{0001}\\ 0 & 0 & 1 & 0\end{bmatrix}. \qquad (16)$$

The matrix A is transformed by

$$\boldsymbol{x} = T\boldsymbol{z} \qquad (17)$$

into

$$B = T^{-1}AT = \begin{bmatrix} \alpha_1 & -\beta_1 & 0 & 0\\ \beta_1 & \alpha_1 & 0 & 0\\ 0 & 0 & \alpha_2 & -\beta_2\\ 0 & 0 & \beta_2 & \alpha_2\end{bmatrix} \qquad (18)$$

where α_i and β_i $(i = 1, 2)$ are the real and imaginary parts of the eigenvalues of the matrix A, respectively. Thus, the nonlinear system (15)

$$\dot{\boldsymbol{x}} = A\boldsymbol{x} + F_{2,3}(\boldsymbol{x}) \qquad (19)$$

is represented by

$$\dot{\boldsymbol{z}} = B\boldsymbol{z} + G_{2,3}(\boldsymbol{z}) \qquad (20)$$

where $F_{2,3}(\boldsymbol{x})$ and $G_{2,3}(\boldsymbol{z})$ include second and third order of polynomials, and $G_{2,3}(\boldsymbol{z}) = T^{-1}F_{2,3}(T\boldsymbol{z})$. Nonlinear structure of the approximate model (20) can be investigated precisely by using a software for nonlinear analysis [10]. Then, one parameter is required for the bifurcation analysis. Here, α_1 is selected as the bifurcation parameter since α_1 corresponds to the damping of the mode which becomes unstable as the power flow increases, where it is supposed that the variation of β_1, α_2, β_2 and the coefficients included in $G_{2,3}(\boldsymbol{z})$ is smaller than that of

α_1 near the Hopf bifurcation. The bifurcation parameter α_1 is related to the input power to the generator P_m linearly as shown in the next section. Thus, the result of the approximate model can be compared with the original model. Transforming the obtained limit cycle of the model (20) by (17), the stable region of the original power system is evaluated.

The procedure of calculation of bifurcation characteristics using a coupled vibration model consists of the following steps.

1) Calculate the participation factors (6) of the linearized system, then select three generators, which participate significantly in the dominant and quasidominant modes, by comparing the factors associated with the rotor angle. One of them is the reference generator, and other two are the analyzed ones.
2) Obtain the oscillation data of these generators by using a power system simulation program.
3) Determine coefficients a_{ijkl} and b_{ijkl} of the coupled vibration model (15) by the least squares method based on obtained data.
4) Calculate the nonlinear structure of the transformed model (20) by using a general software for nonlinear analysis AUTO [10]. The obtained results are transformed again by (17).
5) As a result, the stability and the size of the limit cycle are determined.

In this paper, a coupled vibration model with two dominant electro-mechanical modes associated with angle stability is discussed. Therefore, this method is applicable in the case that a dominant and a quasidominant modes are classified while the generators participating in these modes are specified. A longitudinal interconnected power system is the typical case where these conditions are satisfied. In other cases, for example, a meshed power system, this method may be simply inapplicable. Moreover since it is a method based on the swing equations, it is inapplicable also to the voltage instability phenomenon. On the other hand, this method can be extended to the case expressed in more than two dominant modes. That is, by increasing state variables and choosing the corresponding generators according to the number of the dominant modes. However, the number of the coefficients of nonlinear terms increases enormously and execution becomes practically infeasible.

V. Assessment in a Three-Machine System

The proposed method is applied to a three-machine longitudinally interconnected system. The bifurcation characteristics and the limit cycles of the single and coupled vibration models are compared to those of the original model.

A. Bifurcation Diagram as the Reference

Fig. 2 shows the configuration of the power system model used in this study. The bifurcation characteristics of the system can be calculated correctly as the reference by using a general software for nonlinear analysis AUTO [10], since the example system is relatively simple and small. Table I shows the system constants. The three generators are identical for simplicity. This setting does not lose generality to show a suitable numerical example. Each generator is equipped with an AVR shown in Fig. 3. Here, two cases are considered as shown in Table II, where P_{mi} is the input power to the generator i. An assumed system disturbance is a three phase ground fault at $\times$ near the generator 3.

Here, the generator 1 is selected as the reference of the rotor angle since the dominant oscillation is formed by generators between both ends in a longitudinal system. Figs. 4 and 5 show the bifurcation diagrams depicted by changing the input power to the generator 3 (P_{m3}) as a bifurcation parameter, where the

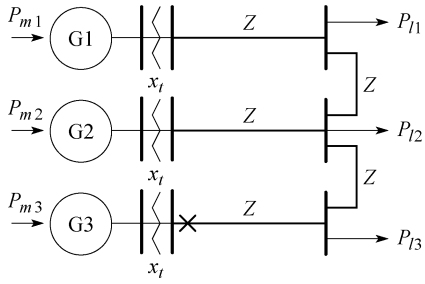

Fig. 2. Three-machine longitudinal power system.

TABLE I
System Constants of Three-Machine System

Generator: Park's 5th model, 4000MVA base		
$x_d = 1.79$ (p.u.)	$x'_d = 0.355$ (p.u.)	$x''_d = 0.275$ (p.u.)
$x_q = 1.66$ (p.u.)	$x'_q = 0.570$ (p.u.)	$x''_q = 0.275$ (p.u.)
$T'_{do} = 7.90$ (s)	$T''_{do} = 0.032$ (s)	$T''_{qo} = 0.410$ (s)
$M = 7.53$ (s)	$D = 0.0$ (s)	$V_{\text{ref}} = 1.0$ (p.u.)
Transmission System: 4000MVA, 500kV base		
$x_t = 0.14$ (p.u.)	$Z = 0.00421 + j0.10$ (p.u.)	

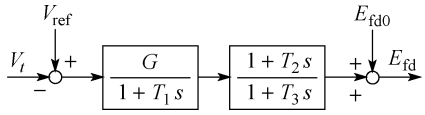

Fig. 3. Block diagram of AVR.

TABLE II
Parameters of AVR and Operating Points

case	G	T_1	T_2	T_3	P_{m1} (p.u.)	P_{m2} (p.u.)	P_{m3} (p.u.)
1	180.0	0.08	0.15	0.80	0.91	0.90	1.29
2	120.0	0.05	0.15	0.30	0.91	1.00	0.95

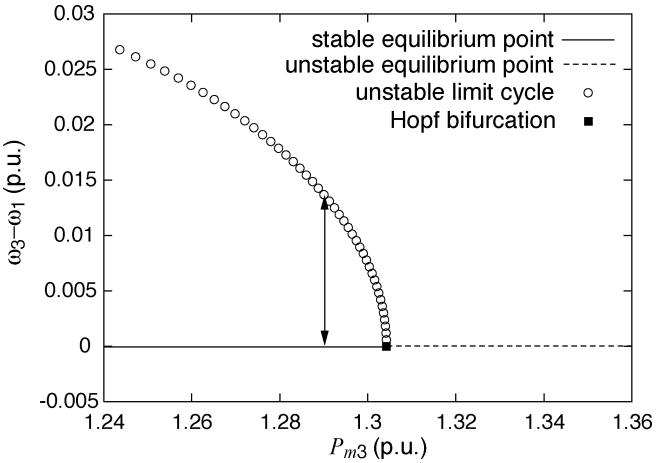

Fig. 4. Bifurcation diagram in case 1.

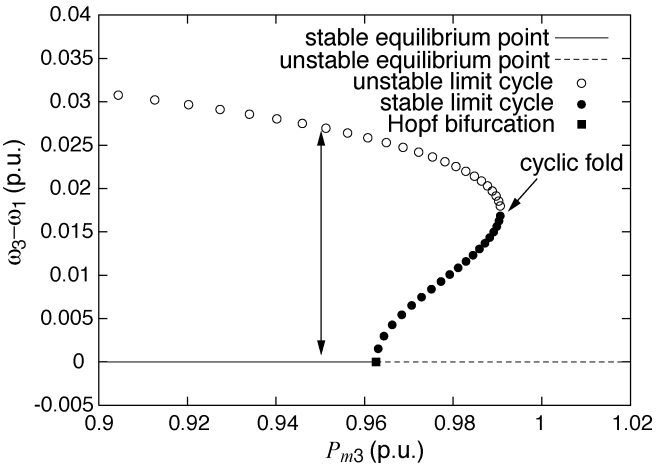

Fig. 5. Bifurcation diagram in case 2.

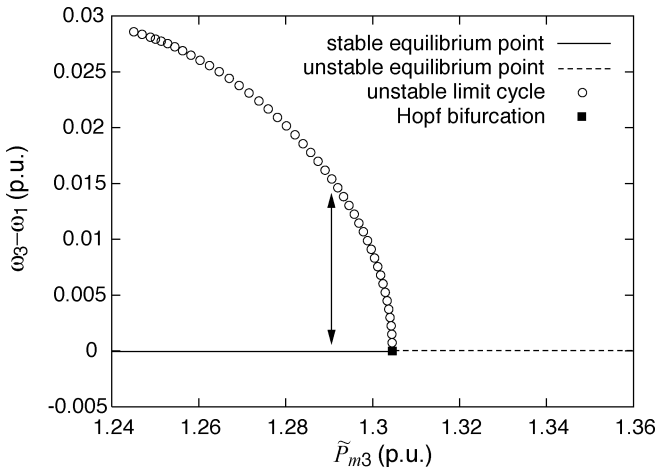

Fig. 6. Bifurcation diagram of the single vibration model in case 1.

TABLE III
THE COEFFICIENTS OF APPROXIMATE MODEL

	case 1	case 2
k_1	-4.435×10^{-2}	-1.924×10^{-2}
k_2	-4.819×10^{1}	-5.633×10^{1}
k_3	-1.173×10^{-1}	-1.520×10^{-2}
k_4	1.627×10^{1}	6.578×10^{-3}
k_5	8.353×10^{-1}	2.920×10^{-2}
k_6	1.312×10^{-3}	1.217×10^{-3}
k_7	5.464	1.996×10^{1}
k_8	-1.940×10^{-1}	4.812×10^{-3}
k_9	-7.774×10^{-2}	-4.748×10^{-1}
residual	1.956×10^{-8}	4.061×10^{-4}
a	0.0740	-0.0674
stability	subcritical	supercritical

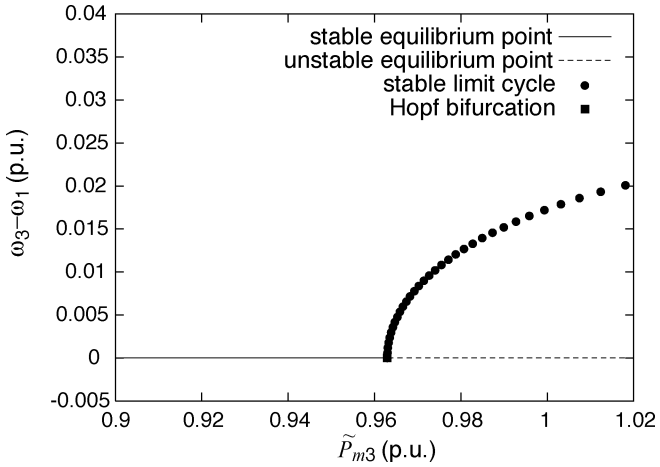

Fig. 7. Bifurcation diagram of the single vibration model in case 2.

limit cycles are represented by the maximum envelop of orbit. In case 1, an unstable limit cycle is formed around the stable equilibrium originating from Hopf bifurcation point at which the stability of the equilibrium point changes from stable to unstable. On the other hand, in case 2 a stable limit cycle is formed around the unstable equilibrium point. However, a cyclic fold bifurcation occurs as the parameter varies. The stability of the limit cycle changes from stable to unstable [8], [9], [16].

Assume that the system is initially operated at the points shown in Table II. These operating points correspond to the slightly stable side of the Hopf bifurcation point. These diagrams show that an unstable limit cycle exists around the operating point, that is, the global stability boundary is determined by this limit cycle. In case 1, the size of the unstable limit cycle at the operating point is $x_{1\max}/(120\pi) = 0.0137$ (p.u.) and $x_{2\max} = 0.785$ (rad). In case 2, the size is $x_{1\max}/(120\pi) = 0.0271$ (p.u.) and $x_{2\max} = 1.396$ (rad).

B. Analysis Using the Single Vibration Model

The nonlinear characteristics of the system are investigated by using the model with a single vibration. Table III shows the coefficients of (9) determined by the least squares method using the system swing data when a three phase ground fault for 0.01 s is applied to the system operated at the points described in Table II. The residual sum of squares in both cases are also shown in Table III. The calculation time for obtaining oscillation data using a power system simulation package comprises a significant percentage of creating the approximate model. However, it does not take so much time. In this case, the CPU time required to obtain the oscillation data is 1.4 s on a PC with Celeron 1.2 GHz. The sign of a calculated by (13) tells us that the system has subcritical Hopf in case 1, and supercritical Hopf in case 2. Figs. 6 and 7 show the bifurcation diagrams of the single vibration models in both cases. These diagrams are depicted by changing k_1 as a parameter. Since $k_1/2$ is the real part of eigenvalues of the linearized system of (9), that is, k_1 corresponds to the system damping. Therefore, it is adequate to select k_1 as a parameter of the single vibration model in the bifurcation analysis.

On the other hand, the parameter of the bifurcation diagram was the mechanical input P_{m3} in the previous section. Thus, the relation between k_1 and P_{m3} is calculated for easy comparison of the results. The eigenvalues have been analyzed by linearizing the original model, then the relation between the real part of the eigenvalues and the mechanical input P_{m3} near the Hopf bifurcation point has been calculated. The relation between k_1 and P_{m3} is determined by the fact that the real part of the eigenvalues is equal to $k_1/2$. Fig. 8 shows the result in case 1. The relation is almost linear. In case 2 the same result was obtained.

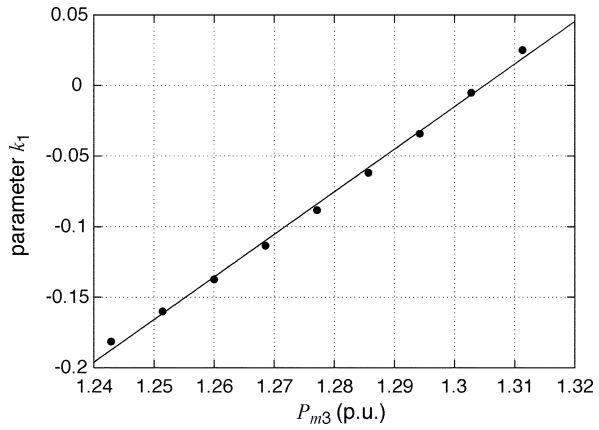

Fig. 8. Relation between the parameter k_1 and the generator input P_{m3}.

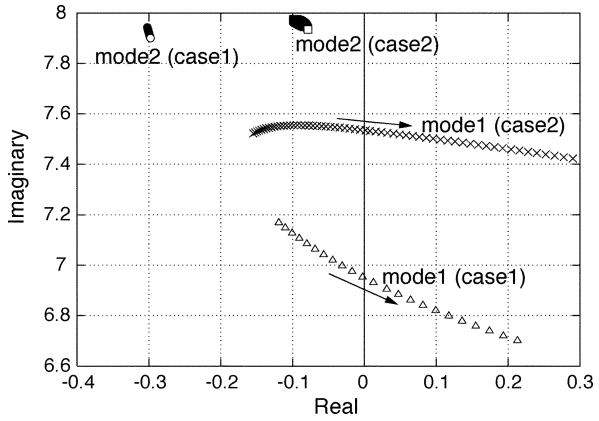

Fig. 9. Variation of eigenvalues when the input power to the generator 3 increases.

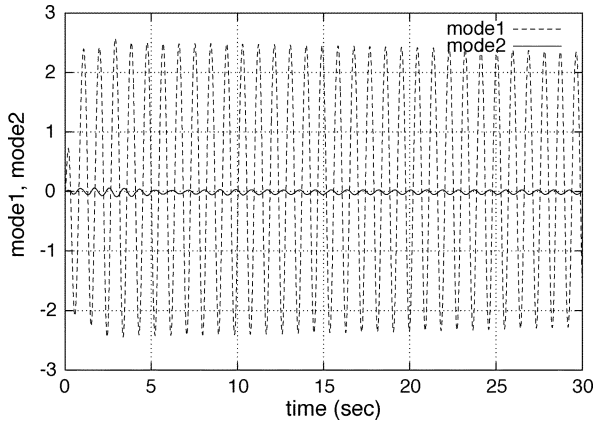

Fig. 10. Mode swing in case 1.

In Figs. 6 and 7, the parameter k_1 has been transformed to P_{m3} by using the linear correlation.

In case 1 the result is correct on the whole. The size of the unstable limit cycle at the operating point can be calculated by (14). The result is $x_{1\max}/(120\pi) = 0.0143\ (\mathrm{p.u.})$ and $x_{2\max} = 0.774\ (\mathrm{rad})$. These values coincide well with those of the original model. The differences between original and approximate models are 4.4% to $x_{1\max}$ and 1.4% to $x_{2\max}$. On the other hand, in case 2 shown in Fig. 7 the fact that a stable

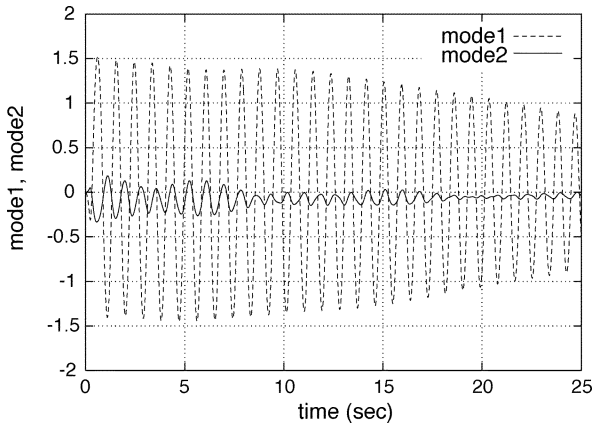

Fig. 11. Mode swing in case 2.

TABLE IV
THE COMPARISON OF RESIDUAL

model (order)	$\dot{x}_1$	$\dot{x}_3$
single (3)	4.061×10^{-4}	1.210×10^{-1}
coupled (3)	1.750×10^{-10}	8.764×10^{-11}
coupled (4)	7.266×10^{-12}	1.546×10^{-12}
coupled (5)	4.254×10^{-14}	5.136×10^{-14}

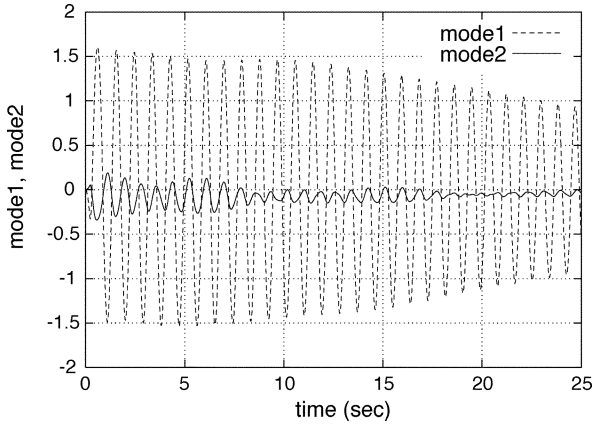

Fig. 12. Mode swing of the approximate model.

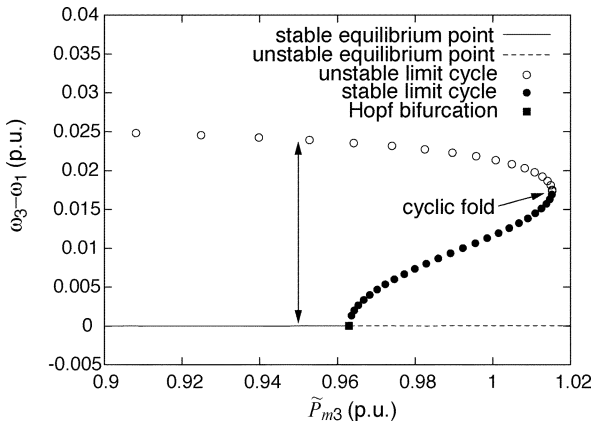

Fig. 13. Bifurcation diagram of the coupled vibration model.

limit cycle exists near the Hopf bifurcation point is correctly derived. However, the characteristics in the region away from the equilibrium point, that is, the existence of an unstable

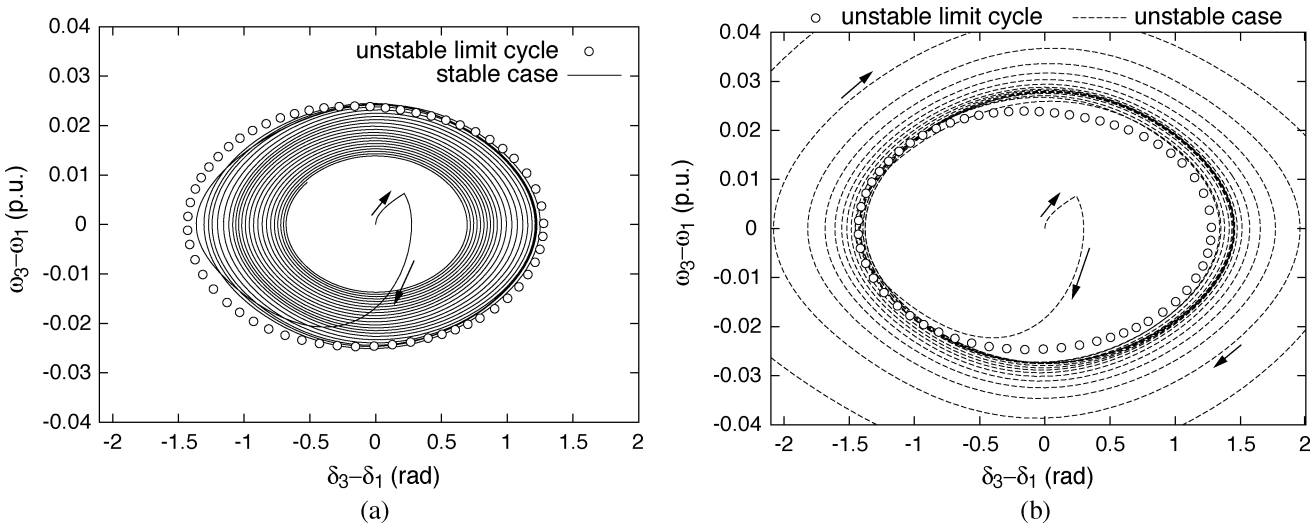

Fig. 14. Unstable limit cycle and system responses on the phase plane. (a) Stable case. (b) Unstable case.

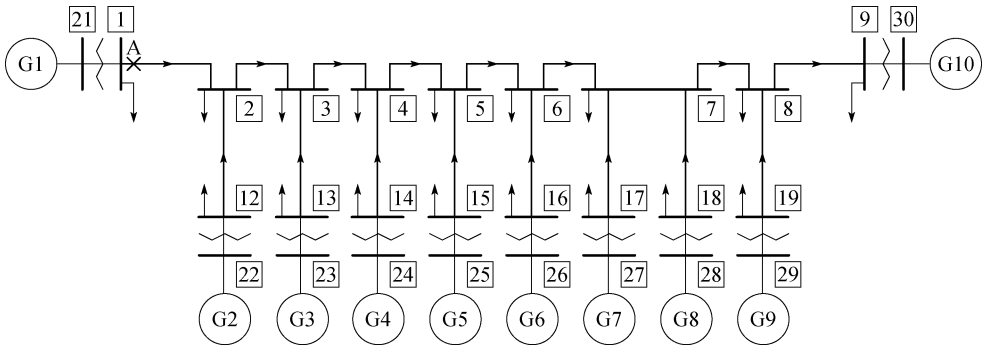

Fig. 15. IEEJ WEST10-machine system model.

limit cycle cannot be evaluated by the single vibration model. The eigenvalues and eigenvectors of the system have been calculated by linearizing the differential equations describing the power system. The result tells us that the generator 3 oscillation mainly participates in the eigenvalue pair closest to the imaginary axis, which we call mode 1, and the generator 2 oscillation mainly participates in the second closest pair, which we call mode 2. Fig. 9 shows the variation of eigenvalues when the input power to the generator 3 increases. In case 1, only mode 1 is dominant. On the other hand, in case 2, the location of mode 2 is very close to the imaginary axis, that is, two modes are easy to interact.

Figs. 10 and 11 show the swing of the two modes decomposed by using the eigenvectors, when the fault is cleared at 0.054 s in case 1 and at 0.2 s in case 2. In Fig. 10, the participation of mode 2 is little. Therefore, the approximation by the single vibration model is satisfactory as shown in Table III. On the other hand, Fig. 11 shows that the influence of mode 2 appears considerably. As a result the single vibration model inherits the error in case 2.

C. Analysis Using the Coupled Vibration Model

The proposed method has been applied to both cases. In case 1, the obtained characteristics have coincided with those of the original model as obtained by using the single vibration model. In case 2, the results have been different considerably from those of applying the single vibration model. Table IV shows the residual in the least squares method when $\dot{x}_1$ and $\dot{x}_3$ are approximated by the single vibration model and by the coupled vibration model. The residual of the coupled vibration model is much smaller than that of the single vibration model. On the other hand, the accuracy of the coupled vibration models with fourth and fifth order of polynomial is not improved so much. Therefore, the coupled vibration model with third order of polynomial proposed in this paper is used in this study.

Fig. 12 shows swings of the modes decomposed by using the eigenvectors of the Jacobian matrix A of model (16). The result reflects the trend shown in Fig. 11, thus the approximate model proficiently represents the interactive characteristics of the original power system. Fig. 13 shows the bifurcation diagram of the approximate model depicted by changing α_1 as a parameter. The bifurcation characteristic of the single vibration model shown in Fig. 7 coincides with the original model around the Hopf bifurcation. However, it has a problem with the stability transition of the limit cycle. On the other hand, as a result of including the modal interaction in the coupled vibration model, the stability transition of limit cycle is correctly reflected, though the cyclic fold is predicted with a certain amount of error. However, it is a significant result that the method using a coupled vibration model can detect the stability transition by a cyclic fold bifurcation as shown in Fig. 13. In particular, unstable limit cycles, which determine the global stability of the system, appear by

TABLE V
SYSTEM CONSTANTS OF WEST10-MACHINE SYSTEM

Generator: Park's 5th model, 1000MVA base		
$x_d = 1.70$ (p.u.)	$x'_d = 0.35$ (p.u.)	$x''_d = 0.25$ (p.u.)
$x_q = 1.70$ (p.u.)	$x'_q = 0.25$ (p.u.)	$M = 7.00$ (s)
$T'_d = 1.00$ (s)	$T''_d = 0.03$ (s)	$T''_q = 0.03$ (s)
Transmission System: 1000MVA, 500kV base		
Impedance: $Z = 0.0042 + j0.126$ (p.u.)/100km		
Electrical charge capacity: $jY/2 = j0.061$ (p.u.)/100km		
Transformer: $x_t = 0.14$ (p.u.)		
Interconnected line: 100km, double circuit		
Line to generator: 50km (G8: 100km), double circuit		

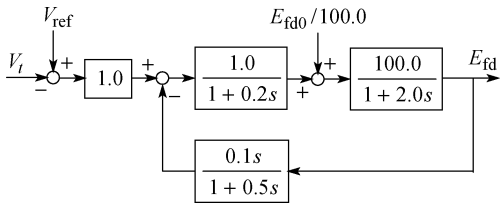

Fig. 16. Block diagram of AVR.

the cyclic fold in this case. It is very important information on the transient stability.

The size of the unstable limit cycle of the approximate model is $x_{1\max}/(120\pi) = 0.025$ (p.u.) and $x_{2\max} = 1.430$ (rad) at the operating point. The differences between original and approximate models are 9.2% to $x_{1\max}$ and 2.4% to $x_{2\max}$. Fig. 14 shows the unstable limit cycle determined by the coupled vibration model and the system responses after the fault projected on the phase plane. When the fault is cleared at 0.2 s, the system state is inside of the limit cycle. The trajectory after the fault converges into the origin. When the fault is cleared at 0.21 s, the system state goes outside of the limit cycle then the generator loses the synchronization. Thus, the stable region is evaluated correctly by this limit cycle. In this case the influence of the modal interaction is properly evaluated by the proposed method based on the coupled vibration model. Note that the state space is of dimension four, therefore the stable manifold of the unstable limit cycle forms the boundary of the global stability in the strict sense. However, as long as the stability associated with the electro-mechanical mode is discussed, the projection of system trajectory on the phase plane gives a good approximation in a physical meaning. Therefore, we discuss the transient stability determined by the limit cycle on the phase plane.

VI. INVESTIGATION IN A TEN-MACHINE SYSTEM

The stable region of IEEJ WEST10-machine system [17] shown in Fig. 15 is investigated. In this case, it is practically impossible to apply a straightforward analysis, that is, to analyze the nonlinear structure of the whole system by using a general software. Therefore, the numerical method proposed in this paper has to be a useful tool for nonlinear structure analysis. Table V shows the system constants. Each generator is equipped with an AVR shown in Fig. 16. The rated capacity and output of the generators are shown in Table VI. In this study, the software for the simulation of power system dynamics, EUROSTAG, is used for the time domain simulation.

TABLE VI
GENERATOR RATED CAPACITY AND OUTPUT

	Capacity (MVA)	Output (MW)
G1	15,000	13,500
G8	5,000	4,500
G10	30,000	27,000
Others	10,000	9,000
Total sum	120,000	108,000

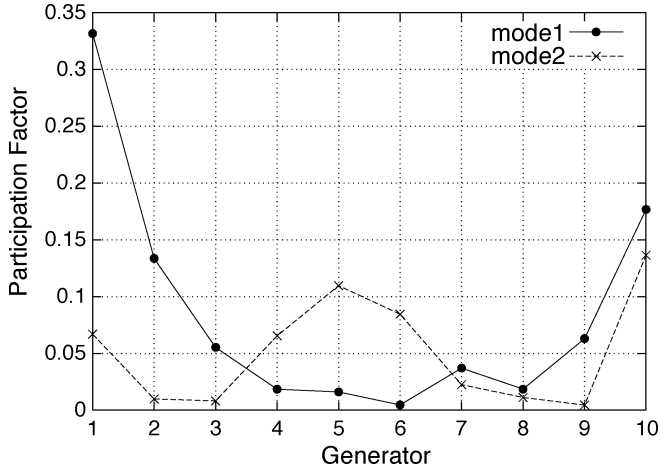

Fig. 17. Participation factors associated with generator angle.

TABLE VII
COMPARISON OF THE RESIDUAL

model (order)	$\dot{x}_1$	$\dot{x}_3$
single (3)	3.868×10^{-1}	1.178×10^{1}
coupled (3)	1.539×10^{-7}	8.399×10^{-8}
coupled (4)	2.616×10^{-8}	1.264×10^{-8}
coupled (5)	2.070×10^{-8}	5.671×10^{-9}

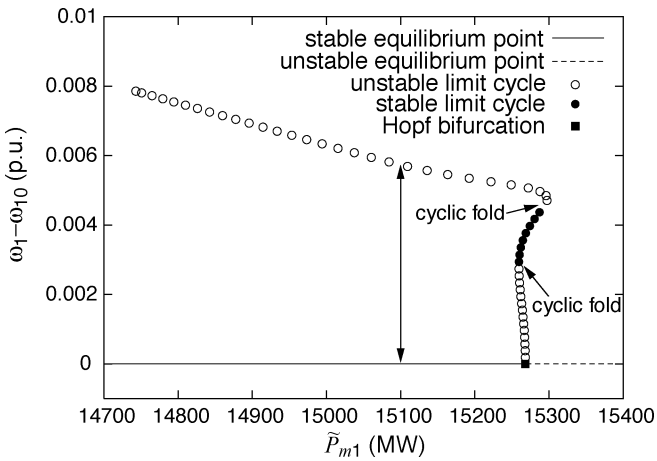

Fig. 18. Bifurcation diagram of the approximate model.

In such a longitudinally interconnected power system, the mode associating with the low-frequency oscillation between both end generators tends to become unstable when the interconnected line is heavily loaded. Here, the load of node 2 and the power of generator 1 are increased by 1600 (MW) so that the line between nodes 1 and 2 is heavi ly loaded. This results

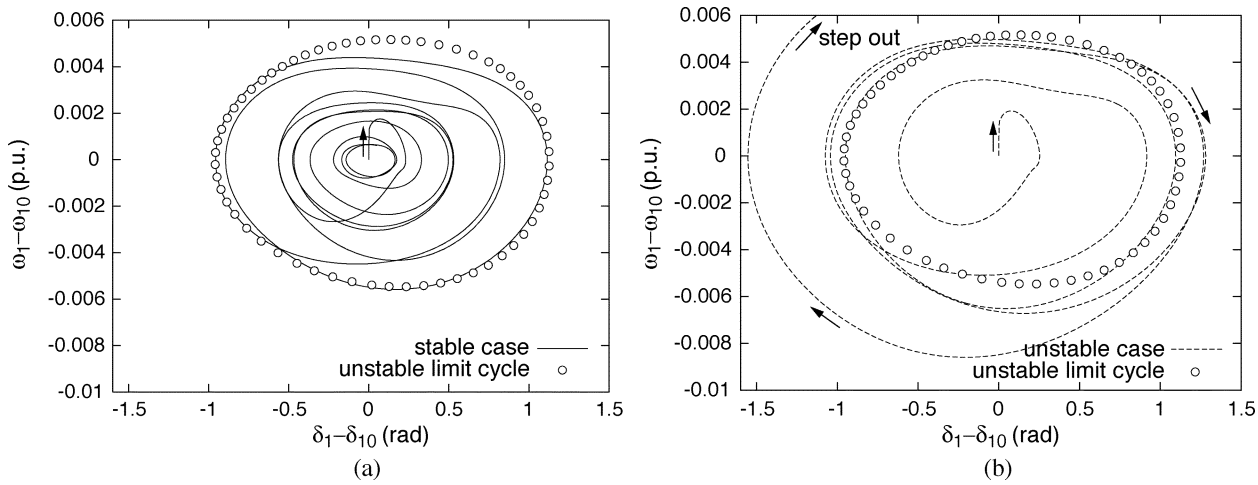

Fig. 19. Unstable limit cycle and system responses on the phase plane. (a) Stable case. (b) Unstable case.

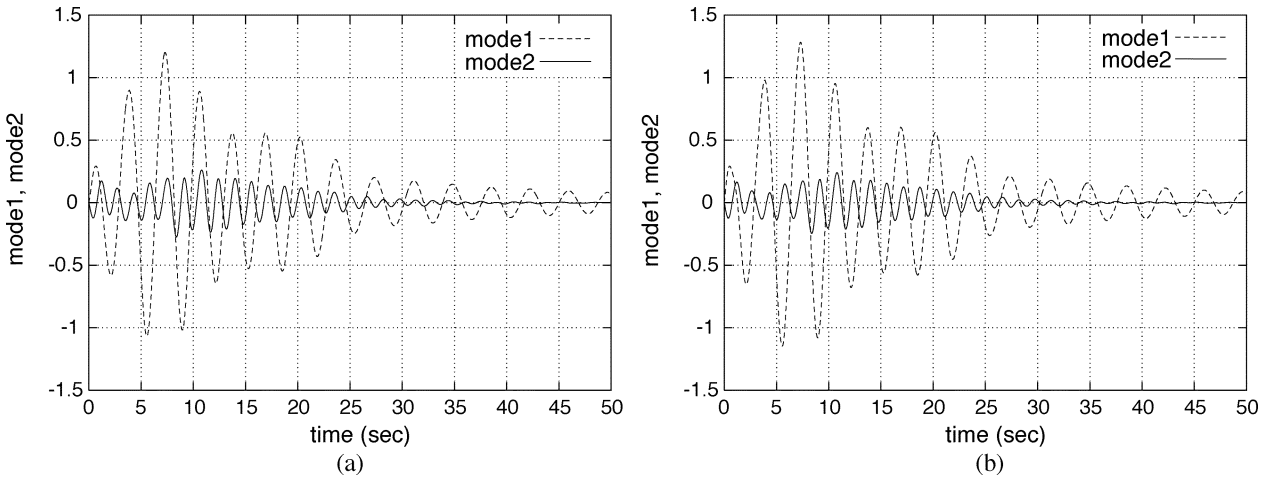

Fig. 20. Comparison of mode swings. (a) Original model. (b) Approximate model.

in the destabilization of the quasidominant mode (mode 2) in addition to the dominant mode (mode 1).

Fig. 17 shows the linear participation factors corresponding to the generator rotor angle. This result shows that generators 1, 5, and 10 participate principally in modes 1 and 2. Therefore, the coupled vibration model is composed of generators 1 and 5 with generator 10 as the reference. In this paper, the linear participation factors corresponding to generator angle are used for selecting generators. In this case, it is sufficient for the following analysis. In a certain kind of case, nonlinear participation factors based on normal form analysis [18] may be needed to evaluate the effective participations, however, the calculation will be quite complicated. Table VII shows the residual in the least squares method, which demonstrates that the coupled vibration model can represent the original dynamics more precisely than the single vibration model.

Figs. 18 and 19 show the bifurcation diagram and the limit cycle on the phase plane, respectively, calculated by using the coupled vibration model. In Fig. 19 the system trajectories are also depicted when the system keeps the stability and when the system becomes unstable, where three phase ground faults cleared at 0.01 s and at 0.011 s are applied, respectively. As shown in the figure, the global stability is bounded by the calculated unstable limit cycle, and the system becomes unstable when the system state moves outside of the limit cycle. Fig. 20 shows swings of the modes decomposed by using the eigenvectors of the original and approximate model, respectively. Each figure coincides well with the other. These results show that the proposed method can evaluate correctly the characteristics around the operating point also in this case.

VII. Conclusion

In this paper, a numerical method to evaluate the Hopf bifurcation characteristics in multi-machine power systems is developed. The single vibration model has been modified to include the modal interaction. The swing equations of two generators significantly participating in dominant and second dominant modes are approximated by a nonlinear coupled vibration model.

The method has been applied to the analysis of nonlinear dynamics in a three-machine longitudinally interconnected power system. The obtained results have been compared to the characteristics of the original model. As a result, it has been seen that the interaction in a coupled vibration model affects the limit cycle significantly. And the characteristics of this model

have coincided well with those of the longitudinal power system model. The method has been also applied to the analysis of the stability associated with a low frequency oscillation in a ten-machine longitudinally interconnected system. Correct evaluation has been demonstrated in numerical studies.

APPENDIX
DERIVATION OF (13) AND (14)

The system (9) changes the stability of equilibrium at $k_1 = 0$, that is, $k_1 = 0$ corresponds to the Hopf bifurcation point. In the following discussion we assume that $k_1 \approx 0$, which corresponds to the status around the Hopf bifurcation. Applying a linear coordinate change of

$$\begin{bmatrix} x_1 \\ x_2 \end{bmatrix} = \begin{bmatrix} \omega & \omega \\ -1 & 1 \end{bmatrix} \begin{bmatrix} z_1 \\ z_2 \end{bmatrix} \tag{21}$$

to (9) at $k_1 = 0$, then

$$\begin{bmatrix} \dot{z}_1 \\ \dot{z}_2 \end{bmatrix} = \begin{bmatrix} 0 & -\omega \\ \omega & 0 \end{bmatrix} \begin{bmatrix} z_1 \\ z_2 \end{bmatrix} + \begin{bmatrix} f^1(z_1, z_2, 0) \\ f^2(z_1, z_2, 0) \end{bmatrix} \tag{22}$$

$$\begin{aligned} f^1 &= f^2 \\ &= (-k_6 + k_7\omega^3 + k_8\omega - k_9\omega^2)z_1^3 \\ &\quad + (k_6 + k_7\omega^3 + k_8\omega + k_9\omega^2)z_2^3 \\ &\quad + (3k_6 + 3k_7\omega^3 - k_8\omega - k_9\omega^2)z_1^2 z_2 \\ &\quad + (-3k_6 + 3k_7\omega^3 - k_8\omega + k_9\omega^2)z_1 z_2^2 \\ &\quad + (k_3 + k_4\omega^2 - k_5\omega)z_1^2 + (k_3 + k_4\omega^2 + k_5\omega)z_2^2 \\ &\quad + (-2k_3 + 2k_4\omega^2)z_1 z_2 \end{aligned} \tag{23}$$

where $\omega = \sqrt{-k_2}$, which is the system angular velocity at $k_1 = 0$. Here, the coefficient a in (4) is related with the nonlinear function in (22) as (see [1])

$$\begin{aligned} a = &\frac{1}{16}\left(f^1_{z_1z_1z_1} + f^1_{z_1z_2z_2} + f^2_{z_1z_1z_2} + f^2_{z_2z_2z_2}\right) \\ &+ \frac{1}{16\omega}\left\{f^1_{z_1z_2}\left(f^1_{z_1z_1} + f^1_{z_2z_2}\right) - f^2_{z_1z_2}\left(f^2_{z_1z_1} + f^2_{z_2z_2}\right)\right. \\ &\left. - f^1_{z_1z_1}f^2_{z_1z_1} + f^1_{z_2z_2}f^2_{z_2z_2}\right\} \end{aligned} \tag{24}$$

where

$$f^l_{z_iz_j} = \frac{\partial^2 f^l}{\partial z_i \partial z_j}(0,0,0), \quad f^l_{z_iz_jz_k} = \frac{\partial^3 f^l}{\partial z_i \partial z_j \partial z_k}(0,0,0).$$

Substituting the detailed form of functions f^1 and f^2 expressed in (23) into (24), a is represented as (13).

In the linearized system of (4), $d\mu$ is the real part of eigenvalue and $k_1/2$ is that in the linearized system of (9). Therefore, the size of limit cycle is written as

$$r = \sqrt{\frac{-k_1}{2a}}. \tag{25}$$

Substituting $z_1 = r\sin\theta$ and $z_2 = r\cos\theta$ into (21), the size of limit cycle is represented as (14).

REFERENCES

[1] J. Guckenheimer and P. Holmes, *Nonlinear Oscillations, Dynamical Systems, and Bifurcations of Vector Fields*. New York: Springer-Verlag, 1983.

[2] S. Wiggins, *Introduction to Applied Nonlinear Dynamical Systems and Chaos*. New York: Springer-Verlag, 1990.

[3] C. D. Vournas *et al.*, "The effect of automatic voltage regulation on the bifurcation evolution in power systems," *IEEE Trans. Power Syst.*, vol. 11, pp. 1683–1688, Nov. 1996.

[4] E. H. Abed and P. P. Varaiya, "Nonlinear oscillations in power systems," *Int. J. Elect. Power Energy Syst.*, vol. 6, no. 1, pp. 37–43, 1984.

[5] V. Ajjarapu and B. Lee, "Bifurcation theory and its application to nonlinear dynamical phenomena in an electrical power system," *IEEE Trans. Power Syst.*, vol. 7, pp. 424–431, Feb. 1992.

[6] J. C. Alexander, "Oscillatory solutions of a model system of nonlinear swing equations," *Int. J. Elect. Power Energy Syst.*, vol. 8, no. 3, pp. 130–136, 1986.

[7] W. D. Rosehart and C. A. Cañizares, "Bifurcation analysis of various power system models," *Int. J. Elect. Power Energy Syst.*, vol. 21, no. 3, pp. 171–182, 1999.

[8] K. G. Rajesh and K. R. Padiyar, "Bifurcation analysis of a three node power system with detailed models," *Int. J. Elect. Power Energy Syst.*, vol. 21, no. 5, pp. 375–393, 1999.

[9] Z. Jing *et al.*, "Bifurcations, chaos, and system collapse in a three node power system," *Int. J. Elect. Power Energy Syst.*, vol. 25, no. 6, pp. 443–461, 2003.

[10] E. J. Doedel *et al.*, "AUTO97: Continuation and Bifurcation Software for Ordinary Differential Equations (With HomCont),", 1997.

[11] Y. Mitani *et al.*, "A numerical method to evaluate bifurcation aspects around generator stability limit," in *Proc. IEEE Int. Symp. Circuits and Systems*, vol. 2, Geneva, Switzerland, May 2000, pp. 565–568.

[12] P. M. Anderson and A. A. Fouad, *Power System Control and Stability*. Ames, IA: The Iowa State Univ. Press, 1977.

[13] I. J. Perez-Arriaga, G. C. Verghese, and F. C. Schweppe, "Selective modal analysis with applications to electric power systems, Part 1: Heuristics introduction," *IEEE Trans. Power Syst.*, vol. PWRS-101, pp. 3117–3125, Sept. 1982.

[14] B. R. Noak *et al.*, "Construction and analysis of differential equations from experimental time series of oscillatory systems," *Physica D: Nonlin. Phenom.*, vol. 56, no. 4, pp. 389–405, 1992.

[15] W. H. Press *et al.*, *Numerical Recipes in C: The Art of Scientific Computing*. Cambridge, U.K.: Cambridge Univ. Press, 1992.

[16] C. W. Tan *et al.*, *Proc. IEEE*, vol. 83, pp. 1484–1496, Nov. 1995.

[17] Technical Committee of IEEJ. (1999) Japanese Power System Models. [Online] Available: http://www.iee.or.jp/pes/model/english/index.html

[18] S. K. Starrett and A. A. Fouad, "Nonlinear measures of mode-machine participation," *IEEE Trans. Power Syst,*, vol. 13, pp. 389–394, May 1998.

Masayuki Watanabe (S'03) received the B.S., M.S., and D.Eng. degrees in Electrical Engineering from Osaka University, Osaka, Japan, in 2001, 2002, and 2004, respectively.

Currently, he is a Research Associate at Funded Research Laboratory (Kyushu Electric Power Company, Inc.), Kyushu Institute of Technology, Fukuoka, Japan. His research interest is in the area of analysis of power systems.

Yasunori Mitani (M'87) received the B.S., M.S., and D.Eng. degrees in electrical engineering from Osaka University, Osaka, Japan, in 1981, 1983, and 1986, respectively.

Currently, he is a Professor at the Department of Electrical, Electronic, and Computer Engineering, Kyushu Institute of Technology, Fukuoka, Japan. He was a Visiting Research Associate at the University of California, Berkeley, from 1994 to 1995. His research interests are in the areas of analysis and control of power systems.

Kiichiro Tsuji (M'74) received the B.S. and M.S. degrees in electrical engineering from Osaka University, Osaka, Japan, in 1966 and 1968, respectively, and the Ph.D. degree in system engineering from Case Western Reserve University, Cleveland, OH, in 1973.

Currently, he is a Professor at the Department of Electrical Engineering, Osaka University. His research interests are in the areas of analysis, planning, and evaluation of energy systems, including electrical power systems.